SAND2016-2979C

Channeled Spectropolarimetry Using Iterative Reconstruction

Dennis J. Lee, Charles F. LaCasse, and Julia M. Craven

Sandia National Laboratories, 1515 Eubank Blvd. SE, Albuquerque, NM 87123

ABSTRACT

Channeled spectropolarimeters (CSP) measure the polarization state of light as a function of wavelength. Conventional Fourier reconstruction suffers from noise, assumes the channels are band-limited, and requires uniformly spaced samples. To address these problems, we propose an iterative reconstruction algorithm. We develop a mathematical model of CSP measurements and minimize a cost function based on this model. We simulate a measured spectrum using example Stokes parameters, from which we compare conventional Fourier reconstruction and iterative reconstruction. Importantly, our iterative approach can reconstruct signals that contain more bandwidth, an advancement over Fourier reconstruction. Our results also show that iterative reconstruction mitigates noise effects, processes non-uniformly spaced samples without interpolation, and more faithfully recovers the ground truth Stokes parameters. This work offers a significant improvement to Fourier reconstruction for channeled spectropolarimetry.

Keywords: Channeled spectropolarimetry, iterative reconstruction, signal processing, Fourier transform, polarimetry, spectroscopy, VNIR, Stokes parameters, dispersive spectrometers, FTIR

1. INTRODUCTION

Channeled spectropolarimetry (CSP) combines the capabilities of polarimetry and spectroscopy. Imaging polarimetry helps to quantify aerosol size distributions, distinguish man-made targets from background clutter, evaluate stress birefringence, and characterize biological tissues.[1] Imaging spectroscopy provides insights in biomedical imaging and remote sensing.[2] Synthesizing these capabilities, CSP has been used to study the polarimetric and ellipsometric properties of dispersive materials.[3,4]

Conventional CSP processing reconstructs Stokes parameters by filtering the Fourier transform of a measured spectrum,[4,5] or by filtering the channeled interferogram if a Fourier transform infrared reflectance (FTIR) instrument is used.[6] There are a few drawbacks to Fourier-based CSP reconstruction:

- It suffers from noise, caused by factors like environmental vibrations, thermal fluctuations, and imperfect sampling.
- It assumes the channels are band-limited. Cross-talk between channels will degrade the reconstruction.
- The Fourier transform requires uniformly spaced samples in wavenumber. A CSP that uses a Fourier transform spectrometer meets this requirement directly, but other spectrometers, such as dispersive based designs, acquire non-uniformly spaced samples in wavenumber. Interpolating samples to a uniform grid introduces errors: Interpolation has to fill in gaps between coarsely spaced samples, while it may discard some finely spaced samples.

  As an aside, despite their drawback of non-uniform sampling, dispersive spectrometers offer advantages for some applications. Compared with a FTIR, they may provide better sampling in the visible and near infrared (VNIR), they may be less sensitive to vibration and environmental noise, and they may be able to better monitor a single IR wavelength to measure the kinetics of a fast chemical reaction.[7]

  On the other hand, a FTIR based approach may offer advantages over dispersive systems. For example, measuring a broad passband is easier, the signal and throughput may be greater, and the design may be easier to modify. This work improves the capabilities of both approaches.

Further author information: (Send correspondence to D.J.L.)
D.J.L.: E-mail: dlee1@sandia.gov

Iterative reconstruction helps to solve these problems. It is a popular technique in x-ray computed tomography (CT), where it helps to lower radiation doses.[8] To our knowledge, this work is the first application of iterative reconstruction to channeled spectropolarimetry. This approach offers multiple advantages:

- It reduces noise from sources like environmental vibrations and thermal fluctuations.
- It doesn't assume the channels are band-limited, which is a common source of error when filtering measurements from modulated polarimeters.[9] Importantly, it can reconstruct signals that contain more bandwidth, an advancement over Fourier reconstruction.
- It can process measurements that are non-uniformly spaced in wavenumber.
- It quantifies reconstruction improvement through minimization of a cost function.

Currently, Fourier reconstruction is the only algorithm for recovering the Stokes parameters from CSP data. In this paper, we will describe how iterative reconstruction can improve Fourier reconstruction for channeled spectropolarimetry.

2. CHANNELED SPECTROPOLARIMETRY SYSTEM

A CSP system typically combines two high-order uniaxial crystal retarders and an analyzer with a spectrometer.[4,10] We will consider the specific system consisting of an achromatic wave plate (QWP), a retarder oriented at 45°, and an analyzer with a spectrometer. The input Stokes parameters are

$$\mathbf{S}_{\text{in}}(\sigma) = \begin{bmatrix} S_0(\sigma) & S_1(\sigma) & S_2(\sigma) & S_3(\sigma) \end{bmatrix}^T, \tag{2.1}$$

and the output Stokes parameters are

$$\mathbf{S}_{\text{out}}(\sigma) = \mathbf{M}_{\text{pol}}\ \mathbf{M}_{45^\circ}(\sigma)\ \mathbf{M}_{\text{QWP}}\ \mathbf{S}_{\text{in}}(\sigma), \tag{2.2}$$

where

$$\mathbf{M}_{\text{pol}} = \begin{bmatrix} 1 & 1 & 0 & 0 \\ 1 & 1 & 0 & 0 \\ 0 & 0 & 0 & 0 \\ 0 & 0 & 0 & 0 \end{bmatrix}, \tag{2.3}$$

$$\mathbf{M}_{45^\circ}(\sigma) = \begin{bmatrix} 1 & 0 & 0 & 0 \\ 0 & \cos(\phi) & 0 & -\sin(\phi) \\ 0 & 0 & 1 & 0 \\ 0 & \sin(\phi) & 0 & \cos(\phi) \end{bmatrix}, \tag{2.4}$$

and

$$\mathbf{M}_{\text{QWP}} = \begin{bmatrix} 1 & 0 & 0 & 0 \\ 0 & 1 & 0 & 0 \\ 0 & 0 & 0 & 1 \\ 0 & 0 & -1 & 0 \end{bmatrix} \tag{2.5}$$

are the Mueller matrices of the polarizer, 45° retarder, and QWP. The spectrometer measures the intensity

$$I(\sigma) = \frac{1}{2}\left\{S_0(\sigma) + S_1(\sigma)\cos[\phi(\sigma)] + S_2(\sigma)\sin[\phi(\sigma)]\right\} \tag{2.6}$$

with phase shift

$$\phi(\sigma) = 2\pi\sigma B(\sigma) l, \tag{2.7}$$

where $\sigma = 1/\lambda$, and $B(\sigma) = |n_o(\sigma) - n_e(\sigma)|$.

In the following two sections, we describe techniques for recovering the Stokes parameters from the measured spectrum in Eq. (2.6). First we review Fourier reconstruction. Then we present iterative reconstruction as an improvement over conventional Fourier processing.

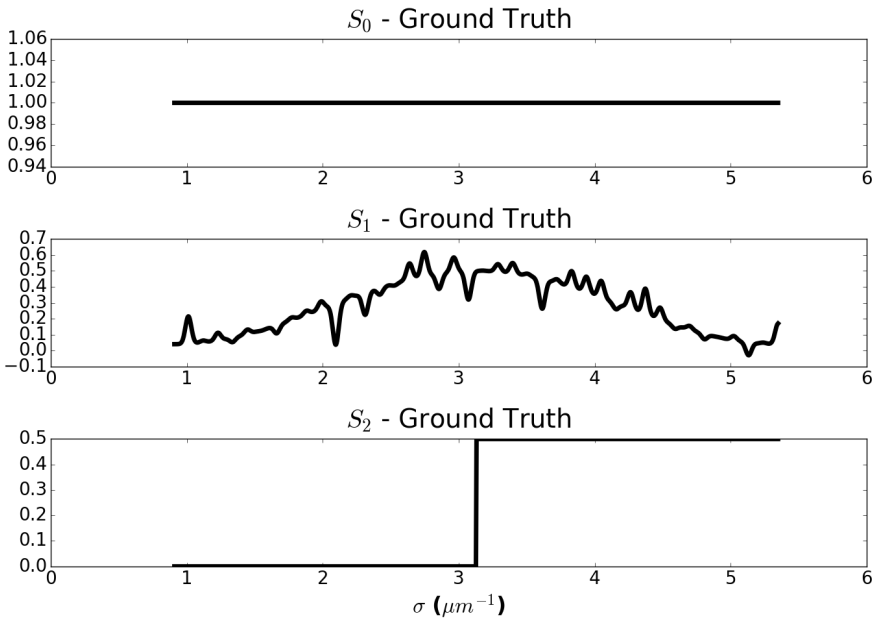

Figure 3.1. Stokes parameters used to simulate the sample spectrum.

3. FOURIER RECONSTRUCTION

The inverse Fourier transform of $I(\sigma)$ separates into channels, from which the Stokes parameters can be recovered. The phase shift $\phi(\sigma)$ affects the channel content, and a reference measurement with a known polarization state characterizes the phase terms.

For simulation, we set values for the Stokes parameters $S_0(\sigma)$, $S_1(\sigma)$, and $S_2(\sigma)$, shown in Figure 3.1. We also set values for the reference parameters: $\tilde{S}_0(\sigma) = 1$, $\tilde{S}_1(\sigma) = 1$, and $\tilde{S}_2(\sigma) = 0$ for all σ.

Using these Stokes parameters, we can simulate measurements of the sample and reference spectra according to Eq. (2.6), shown in Fig. 3.2. We add noise to the simulated spectra, described in detail later; Eqs. (4.18)–(4.19) describe the Gaussian noise model, and Eqs. (5.1)–(5.2) specify the mean and standard deviation. The simulated Stokes parameters and spectra are non-uniformly spaced in wavenumber to emulate measurements from a dispersive spectrometer. The goal is to reconstruct $S_0(\sigma)$, $S_1(\sigma)$, and $S_2(\sigma)$ from these simulated measurements. Fourier reconstruction proceeds according to the following steps:

1. Inverse Fourier transform the sample and reference spectra (Fig. 3.2), which are functions of wavenumber, to obtain interferograms. We interpolate the spectra to be uniformly spaced along wavenumber before the Fourier transform.

2. Separate the interferogram into channels: $C_0(d)$ and $C_1(d)$ for the sample signal, and $\tilde{C}_0(d)$ and $\tilde{C}_1(d)$ for the reference signal, where d is the optical path delay (OPD). Figure 3.3 depicts interferograms with Hamming filters overlaid. Multiplying each interferogram by the green and blue Hamming filters isolates channels 0 and 1, respectively.

3. Compute the Stokes parameters by processing the Fourier transform of the channels:

$$S_0(\sigma) = \left|\mathcal{F}\left[C_0(d)\right](\sigma)\right|. \tag{3.1}$$

The Fourier transform of $\tilde{C}_1(d)$ contains information on the dispersion and linear phase shifts in $C_1(d)$. For phase correction, we extract the phase of the reference signal for channel 1,

$$\tilde{\phi}_1(\sigma) = \arg\left\{\ \mathcal{F}\left[\tilde{C}_1(d)\right](\sigma)\right\}. \tag{3.2}$$

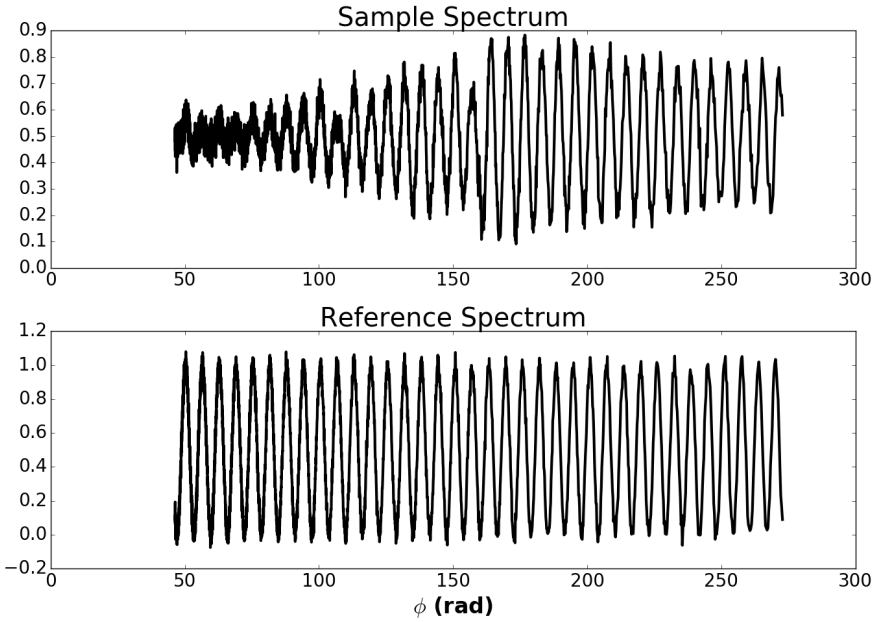

Figure 3.2. Simulated measurements of the sample (top) and reference (bottom) spectra.

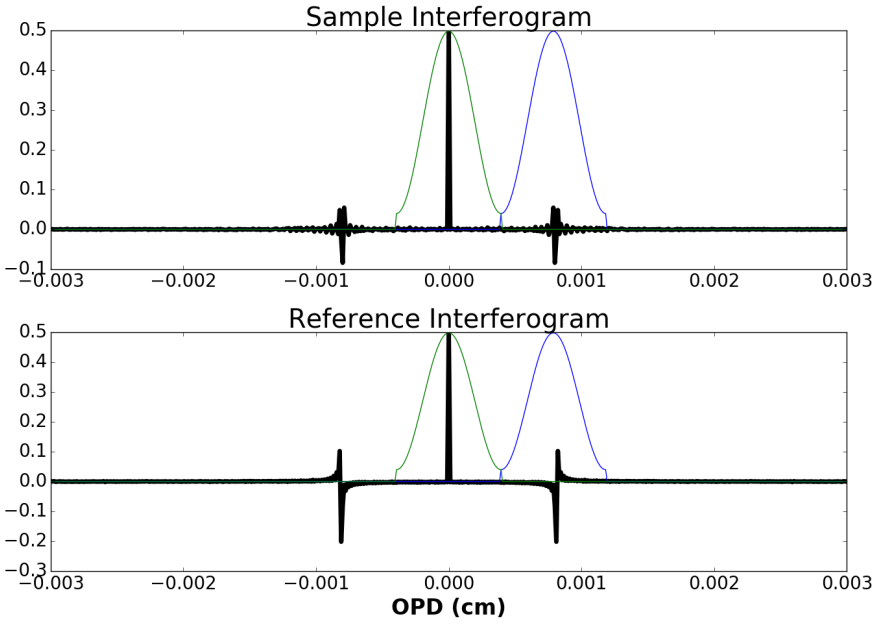

Figure 3.3. Interferograms of the sample (top) and reference (bottom) signals.

We compute $S_1(\sigma)$ and $S_2(\sigma)$ using this phase correction:

$$S_1(\sigma) = \mathrm{Re}\left\{\mathcal{F}\left[C_1(d)\right](\sigma) \cdot e^{-i\tilde{\phi}_1(\sigma)}\right\} \tag{3.3}$$

and

$$S_2(\sigma) = \mathrm{Im}\left\{\mathcal{F}\left[C_1(d)\right](\sigma) \cdot e^{-i\tilde{\phi}_1(\sigma)}\right\}. \tag{3.4}$$

Figure 3.4 shows the recovered Stokes parameters for our simulation. We plot the absolute difference between the ground truth and reconstruction, with the root mean squared error (RMSE) displayed to quantify error. In the next section, we will develop a different reconstruction technique to improve these results.

4. ITERATIVE RECONSTRUCTION

4.1 Continuous Model

Ideally, a CSP system measures a noiseless intensity, modeled as

$$I_{\text{model}}(\sigma) = \frac{1}{2}\left\{S_0(\sigma) + S_1(\sigma)\cos[\phi(\sigma)] + S_2(\sigma)\sin[\phi(\sigma)]\right\}. \tag{4.1}$$

We can approximate noise as Gaussian, which corrupts the model $I_{\text{model}}(\sigma)$. Let $I(\sigma)$ denote the measured, noisy intensity:

$$I(\sigma) = I_{\text{model}}(\sigma) + n. \tag{4.2}$$

We assume that the noise follows an independent, identically distributed Gaussian distribution,

$$n \sim \mathcal{N}\left(\mu, \sigma_n^2\right), \tag{4.3}$$

with mean μ and variance σ_n^2. We formulate the problem as the minimization of a cost function with the general form

$$c(S_0, S_1, S_2) = L(S_0, S_1, S_2) + \beta_0 R_0(S_0) + \beta_1 R_1(S_1) + \beta_2 R_2(S_2) \tag{4.4}$$

where $L(S_0, S_1, S_2)$ is the negative log-likelihood function corresponding to our model of the noisy measurements as a Gaussian distribution, β_0, β_1 and β_2 are scalar regularization parameters, and $R_0(S_0)$, $R_1(S_1)$, and $R_2(S_2)$ are roughness penalty functions for S_0, S_1, and S_2, respectively. Note that we suppress functional dependence on wavenumber σ for ease of notation.

In the continuous formulation, the likelihood function has the form

$$L(S_0, S_1, S_2) = \frac{1}{2}\int_{\mathbb{R}} \left[\frac{1}{2}\left\{S_0(\sigma) + S_1(\sigma)\cos[\phi(\sigma)] + S_2(\sigma)\sin[\phi(\sigma)]\right\} - I(\sigma)\right]^2 d\sigma, \tag{4.5}$$

which measures the difference between our model $I_{\text{model}}(\sigma)$ and the data $I(\sigma)$. To reduce noise, or penalize roughness, and impose constraints like edge-preserving smoothness on our signals, we minimize the total variation of the Stokes parameters with the regularizer terms

$$R_0(S_0) = \int_{\mathbb{R}} \sqrt{|\nabla S_0(\sigma)|^2 + \epsilon}\, d\sigma, \tag{4.6}$$

$$R_1(S_1) = \int_{\mathbb{R}} \sqrt{|\nabla S_1(\sigma)|^2 + \epsilon}\, d\sigma, \tag{4.7}$$

and

$$R_2(S_2) = \int_{\mathbb{R}} \sqrt{|\nabla S_2(\sigma)|^2 + \epsilon}\, d\sigma, \tag{4.8}$$

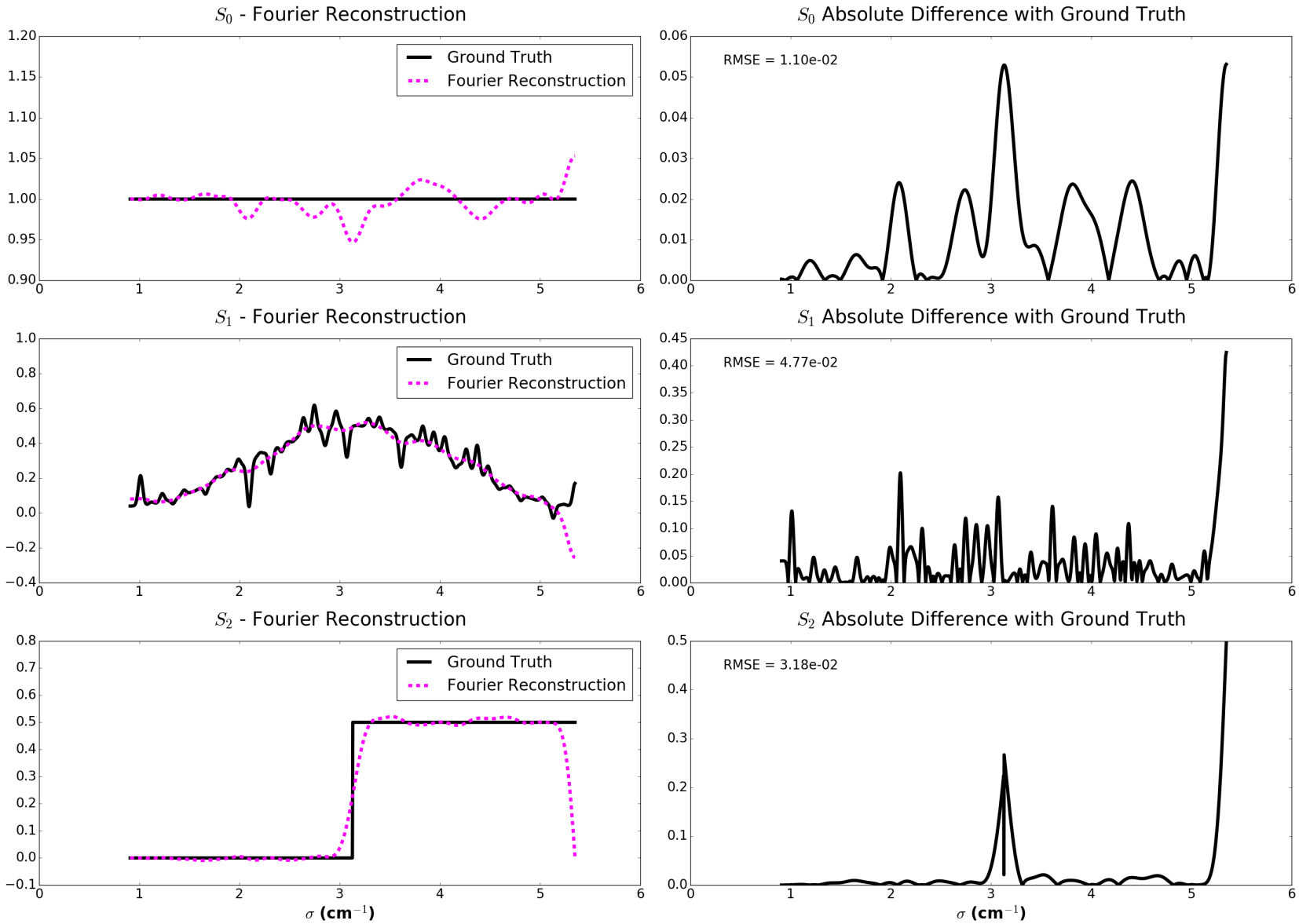

Figure 3.4. Recovered Stokes parameters using Fourier reconstruction

where ϵ is a small constant to ensure differentiability. Now the cost function becomes

$$\begin{aligned} c(S_0, S_1, S_2) &= L(S_0, S_1, S_2) + \beta_0 R_0(S_0) + \beta_1 R_1(S_1) + \beta_2 R_2(S_2) \\ &= \frac{1}{2} \int_{\mathbb{R}} \left[\frac{1}{2} \left\{ S_0(\sigma) + S_1(\sigma) \cos[\phi(\sigma)] + S_2(\sigma) \sin[\phi(\sigma)] \right\} - I(\sigma) \right]^2 d\sigma \\ &+ \beta_0 \int_{\mathbb{R}} \sqrt{|\nabla S_0(\sigma)|^2 + \epsilon}\, d\sigma + \beta_1 \int_{\mathbb{R}} \sqrt{|\nabla S_1(\sigma)|^2 + \epsilon}\, d\sigma + \beta_2 \int_{\mathbb{R}} \sqrt{|\nabla S_2(\sigma)|^2 + \epsilon}\, d\sigma. \end{aligned} \tag{4.9}$$

We aim to solve for the Stokes parameters by minimizing this cost function:

$$\left(\hat{S}_0, \hat{S}_1, \hat{S}_2 \right) = \underset{S_0, S_1, S_2}{\operatorname{argmin}}\, c(S_0, S_1, S_2) \tag{4.10}$$

4.2 Discrete Model

Our goal is to recover the spectrally dependent Stokes parameters. The spectrometer discretizes measurements according to its pixel pitch. If a dispersive spectrometer is used, the wavenumbers σ_i, $i = 1, \ldots, N$, will be non-uniformly spaced, according to the relationship $\sigma = 1/\lambda$. We can represent the sampled wavenumbers as a vector,

$$\sigma = \begin{bmatrix} \sigma_1 & \ldots & \sigma_i & \ldots & \sigma_N \end{bmatrix}^T. \tag{4.11}$$

We write the Stokes parameters as vectors:

$$\mathbf{S}_0(\sigma) = \begin{bmatrix} S_{0,1} & \ldots & S_{0,i} & \ldots & S_{0,N} \end{bmatrix}^T, \tag{4.12}$$

$$\mathbf{S}_1(\sigma) = \begin{bmatrix} S_{1,1} & \ldots & S_{1,i} & \ldots & S_{1,N} \end{bmatrix}^T, \tag{4.13}$$

and

$$\mathbf{S}_2(\sigma) = \begin{bmatrix} S_{2,1} & \ldots & S_{2,i} & \ldots & S_{2,N} \end{bmatrix}^T, \tag{4.14}$$

where N is the number of wavelengths or wavenumbers measured. Similarly, we write the measured intensity as a vector

$$\mathbf{I}(\sigma) = \begin{bmatrix} I_1 & \ldots & I_i & \ldots & I_N \end{bmatrix}^T \tag{4.15}$$

and the phase as a vector

$$\phi(\sigma) = \begin{bmatrix} \phi_1 & \ldots & \phi_i & \ldots & \phi_N \end{bmatrix}^T. \tag{4.16}$$

With this notation, we model the ideal, noiseless measurements as

$$I_i^{\text{model}} = \frac{1}{2} \left[S_{0,i} + S_{1,i} \cos(\phi_i) + S_{2,i} \sin(\phi_i) \right]. \tag{4.17}$$

We can approximate noise in the measured intensity I_i as Gaussian, which causes deviations from the noiseless model I_i^{model} in Eq. (4.17):

$$I_i = I_i^{\text{model}} + n_i. \tag{4.18}$$

We assume that the noise follows an independent, identically distributed Gaussian distribution,

$$n_i \sim \mathcal{N}\left(\mu, \sigma_n^2\right), \tag{4.19}$$

with mean μ and variance σ_n^2. We specify the sampled likelihood function as

$$\begin{aligned} L(\mathbf{S}_0, \mathbf{S}_1, \mathbf{S}_2) &= \frac{1}{2} \sum_{i=1}^{N} \left[\frac{1}{2} \left\{ S_0(\sigma) + S_1(\sigma) \cos[\phi(\sigma)] + S_2(\sigma) \sin[\phi(\sigma)] \right\} - I(\sigma) \right]^2 \Bigg|_{\sigma=\sigma_i} \\ &= \frac{1}{2} \sum_{i=1}^{N} \left\{ \frac{1}{2} \left[S_{0,i} + S_{1,i} \cos(\phi_i) + S_{2,i} \sin(\phi_i) \right] - I_i \right\}^2. \end{aligned} \tag{4.20}$$

Analogous to Eqs. (4.6)–(4.8), we regularize the unknowns by minimizing their total variation, with

$$R_0(\mathbf{S}_0) = \sum_{i=1}^{N} \sqrt{(\mathbf{D}\mathbf{S}_0)_i^2 + \epsilon}, \tag{4.21}$$

$$R_1(\mathbf{S}_1) = \sum_{i=1}^{N} \sqrt{(\mathbf{D}\mathbf{S}_1)_i^2 + \epsilon}, \tag{4.22}$$

and

$$R_2(\mathbf{S}_2) = \sum_{i=1}^{N} \sqrt{(\mathbf{D}\mathbf{S}_2)_i^2 + \epsilon}. \tag{4.23}$$

Here $\mathbf{D}$ is a finite difference matrix implementing the discretized first derivatives using nearest neighbors. The cost function becomes

$$\begin{aligned} c(\mathbf{S}_0, \mathbf{S}_1, \mathbf{S}_2) &= L(\mathbf{S}_0, \mathbf{S}_1, \mathbf{S}_2) + \beta_0 R_0(\mathbf{S}_0) + \beta_1 R_1(\mathbf{S}_1) + \beta_2 R_2(\mathbf{S}_2) \\ &= \frac{1}{2} \sum_{i=1}^{N} \left\{ \frac{1}{2} \left[S_{0,i} + S_{1,i} \cos(\phi_i) + S_{2,i} \sin(\phi_i) \right] - I_i \right\}^2 \\ &+ \beta_0 \sum_{i=1}^{N} \sqrt{(\mathbf{D}\mathbf{S}_0)_i^2 + \epsilon} + \beta_1 \sum_{i=1}^{N} \sqrt{(\mathbf{D}\mathbf{S}_1)_i^2 + \epsilon} + \beta_2 \sum_{i=1}^{N} \sqrt{(\mathbf{D}\mathbf{S}_2)_i^2 + \epsilon}. \end{aligned} \tag{4.24}$$

Our goal is to recover $\mathbf{S}_0$, $\mathbf{S}_1$, and $\mathbf{S}_2$ by minimizing this cost function:

$$\left(\hat{\mathbf{S}}_0, \hat{\mathbf{S}}_1, \hat{\mathbf{S}}_2\right) = \underset{\mathbf{S}_0, \mathbf{S}_1, \mathbf{S}_2 \in \mathbb{R}^N}{\operatorname{argmin}} c(\mathbf{S}_0, \mathbf{S}_1, \mathbf{S}_2). \tag{4.25}$$

We estimate the Stokes parameters by alternating updates in each iteration, a useful technique to solve for multiple unknowns:[11]

$$\mathbf{S}_0^{(n+1)} = \underset{\mathbf{S}_0 \in \mathbb{R}^N}{\operatorname{argmin}}\, c\left(\mathbf{S}_0,\ \mathbf{S}_1^{(n)},\ \mathbf{S}_2^{(n)}\right), \tag{4.26}$$

$$\mathbf{S}_1^{(n+1)} = \underset{\mathbf{S}_1 \in \mathbb{R}^N}{\operatorname{argmin}}\, c\left(\mathbf{S}_0^{(n+1)},\ \mathbf{S}_1,\ \mathbf{S}_2^{(n)}\right), \tag{4.27}$$

and

$$\mathbf{S}_2^{(n+1)} = \underset{\mathbf{S}_2 \in \mathbb{R}^N}{\operatorname{argmin}}\, c\left(\mathbf{S}_0^{(n+1)},\ \mathbf{S}_1^{(n+1)},\ \mathbf{S}_2\right). \tag{4.28}$$

4.3 Iterative Reconstruction Algorithm

To solve the reconstruction problem in Eq. (4.25), we employ the alternating update strategy in Eqs. (4.26)–(4.28), where we use gradient descent for each update. Other optimization algorithms are possible.[12] Gradient descent minimizes a cost function based on computing its gradient, then updating parameters of interest by moving in the opposite direction. For example, to solve for $\mathbf{S}_0$ in Eq. (4.26), at the ith iteration of gradient descent, we move in the direction

$$\begin{aligned} \mathbf{d} &= -\nabla_{\mathbf{S}_0} c\left(\mathbf{S}_0, \mathbf{S}_1, \mathbf{S}_2\right)\big|_{\mathbf{S}_0 = \mathbf{S}_0^{(i)}} \\ &= -\nabla_{\mathbf{S}_0} L\left(\mathbf{S}_0, \mathbf{S}_1, \mathbf{S}_2\right)\big|_{\mathbf{S}_0 = \mathbf{S}_0^{(i)}} - \beta_0 \nabla_{\mathbf{S}_0} R_0\left(\mathbf{S}_0\right)\Big|_{\mathbf{S}_0 = \mathbf{S}_0^{(i)}} \end{aligned} \tag{4.29}$$

and update $\mathbf{S}_0$ according to

$$\mathbf{S}_0^{(i+1)} = \mathbf{S}_0^{(i)} + \alpha^* \mathbf{d}, \tag{4.30}$$

where the step size

$$\alpha^* = \underset{\alpha \in \mathbb{R}}{\operatorname{argmin}}\ c\left(\mathbf{S}_0^{(i)} + \alpha \mathbf{d}, \mathbf{S}_1, \mathbf{S}_2\right) \tag{4.31}$$

Algorithm 4.1 Update S_0 using gradient descent

function UPDATE_S_0 ($\mathbf{S}_0^{\text{in}}$, $\mathbf{S}_1$, $\mathbf{S}_2$)

/* This function computes $\mathbf{S}_0^{\text{out}} = \text{argmin}_{\mathbf{S}_0 \in \mathbb{R}^N} c(\mathbf{S}_0, \mathbf{S}_1, \mathbf{S}_2)$ */

$\mathbf{S}_0^{(0)} \leftarrow \mathbf{S}_0^{\text{in}}$
$i \leftarrow 0$
while $c\left(\mathbf{S}_0^{(i)}, \mathbf{S}_1, \mathbf{S}_2\right) > \epsilon$ **do**
  $\mathbf{d} \leftarrow -\nabla_{\mathbf{S}_0} c(\mathbf{S}_0, \mathbf{S}_1, \mathbf{S}_2)|_{\mathbf{S}_0 = \mathbf{S}_0^{(i)}}$
    $= -\nabla_{\mathbf{S}_0} L(\mathbf{S}_0, \mathbf{S}_1, \mathbf{S}_2)|_{\mathbf{S}_0 = \mathbf{S}_0^{(i)}} - \beta_0 \nabla_{\mathbf{S}_0} R_0(\mathbf{S}_0)\Big|_{\mathbf{S}_0 = \mathbf{S}_0^{(i)}}$
  $\alpha^* \leftarrow \text{argmin}_{\alpha \in \mathbb{R}} \; c\left(\mathbf{S}_0^{(i)} + \alpha \mathbf{d}, \mathbf{S}_1, \mathbf{S}_2\right)$
  $\mathbf{S}_0^{(i+1)} \leftarrow \mathbf{S}_0^{(i)} + \alpha^* \mathbf{d}$
  $i \leftarrow i + 1$
end while

$\mathbf{S}_0^{\text{out}} \leftarrow \mathbf{S}_0^{(i)}$
return $\mathbf{S}_0^{\text{out}}$
end function

Algorithm 4.2 Update S_1 using gradient descent

function UPDATE_S_1 ($\mathbf{S}_0$, $\mathbf{S}_1^{\text{in}}$, $\mathbf{S}_2$)

/* This function computes $\mathbf{S}_1^{\text{out}} = \text{argmin}_{\mathbf{S}_1 \in \mathbb{R}^N} c(\mathbf{S}_0, \mathbf{S}_1, \mathbf{S}_2)$ */

$\mathbf{S}_1^{(0)} \leftarrow \mathbf{S}_1^{\text{in}}$
$i \leftarrow 0$
while $c\left(\mathbf{S}_0, \mathbf{S}_1^{(i)}, \mathbf{S}_2\right) > \epsilon$ **do**
  $\mathbf{d} \leftarrow -\nabla_{\mathbf{S}_1} c(\mathbf{S}_0, \mathbf{S}_1, \mathbf{S}_2)|_{\mathbf{S}_1 = \mathbf{S}_1^{(i)}}$
    $= -\nabla_{\mathbf{S}_1} L(\mathbf{S}_0, \mathbf{S}_1, \mathbf{S}_2)|_{\mathbf{S}_1 = \mathbf{S}_1^{(i)}} - \beta_1 \nabla_{\mathbf{S}_1} R_1(\mathbf{S}_1)\Big|_{\mathbf{S}_1 = \mathbf{S}_1^{(i)}}$
  $\alpha^* \leftarrow \text{argmin}_{\alpha \in \mathbb{R}} \; c\left(\mathbf{S}_0, \mathbf{S}_1^{(i)} + \alpha \mathbf{d}, \mathbf{S}_2\right)$
  $\mathbf{S}_1^{(i+1)} \leftarrow \mathbf{S}_1^{(i)} + \alpha^* \mathbf{d}$
  $i \leftarrow i + 1$
end while

$\mathbf{S}_1^{\text{out}} \leftarrow \mathbf{S}_1^{(i)}$
return $\mathbf{S}_1^{\text{out}}$
end function

can be found using standard line search algorithms.[12] We repeatedly update $\mathbf{S}_0$ according to Eqs. (4.29)–(4.31) until the cost $c(\mathbf{S}_0, \mathbf{S}_1, \mathbf{S}_2)$ reduces below a specified threshold. Algorithm 4.1 describes the update in detail. Once $\mathbf{S}_0$ is updated, we follow an analogous procedure for $\mathbf{S}_1$ and $\mathbf{S}_2$, elaborated in Algorithms 4.2 and 4.3.

These algorithms require the computation of various derivatives. For reference, we list the gradients of the likelihood functions,

$$[\nabla_{\mathbf{S}_0} L(\mathbf{S}_0, \mathbf{S}_1, \mathbf{S}_2, \phi)]_i = S_{0,i} + S_{1,i} \cos(\phi_i) + S_{2,i} \sin(\phi_i) - I_i, \tag{4.32}$$

$$[\nabla_{\mathbf{S}_1} L(\mathbf{S}_0, \mathbf{S}_1, \mathbf{S}_2, \phi)]_i = [S_{0,i} + S_{1,i} \cos(\phi_i) + S_{2,i} \sin(\phi_i) - I_i] \cdot \cos(\phi_i), \tag{4.33}$$

and

$$[\nabla_{\mathbf{S}_2} L(\mathbf{S}_0, \mathbf{S}_1, \mathbf{S}_2, \phi)]_i = [S_{0,i} + S_{1,i} \cos(\phi_i) + S_{2,i} \sin(\phi_i) - I_i] \cdot \sin(\phi_i), \tag{4.34}$$

Algorithm 4.3 Update S_2 using gradient descent

function UPDATE_S_2 ($\mathbf{S}_0$, $\mathbf{S}_1$, $\mathbf{S}_2^{\text{in}}$)

/* This function computes $\mathbf{S}_2^{\text{out}} = \text{argmin}_{\mathbf{S}_2 \in \mathbb{R}^N} c(\mathbf{S}_0, \mathbf{S}_1, \mathbf{S}_2)$ */

$\mathbf{S}_2^{(0)} \leftarrow \mathbf{S}_2^{\text{in}}$
$i \leftarrow 0$
while $c\left(\mathbf{S}_0, \mathbf{S}_1, \mathbf{S}_2^{(i)}\right) > \epsilon$ **do**
  $\mathbf{d} \leftarrow -\nabla_{\mathbf{S}_2} c(\mathbf{S}_0, \mathbf{S}_1, \mathbf{S}_2)|_{\mathbf{S}_2 = \mathbf{S}_2^{(i)}}$
    $= -\nabla_{\mathbf{S}_2} L(\mathbf{S}_0, \mathbf{S}_1, \mathbf{S}_2)|_{\mathbf{S}_2 = \mathbf{S}_2^{(i)}} - \beta_2 \nabla_{\mathbf{S}_2} R_2(\mathbf{S}_2)\Big|_{\mathbf{S}_2 = \mathbf{S}_2^{(i)}}$
  $\alpha^* \leftarrow \text{argmin}_{\alpha \in \mathbb{R}} \; c\left(\mathbf{S}_0, \mathbf{S}_1, \mathbf{S}_2^{(i)} + \alpha \mathbf{d}\right)$
  $\mathbf{S}_2^{(i+1)} \leftarrow \mathbf{S}_2^{(i)} + \alpha^* \mathbf{d}$
  $i \leftarrow i + 1$
end while

$\mathbf{S}_2^{\text{out}} \leftarrow \mathbf{S}_2^{(i)}$
return $\mathbf{S}_2^{\text{out}}$
end function

Algorithm 4.4 Iterative Reconstruction for Channeled Spectropolarimetry

Input: Measured spectrum $\mathbf{I}(\sigma)$
Outputs: Stokes parameters $\mathbf{S}_0$, $\mathbf{S}_1$, $\mathbf{S}_2$

Initialize $\mathbf{S}_0^{(0)}$, $\mathbf{S}_1^{(0)}$, $\mathbf{S}_2^{(0)}$ by Fourier reconstruction.
$n \leftarrow 0$
while $c\left(\mathbf{S}_0^{(n)}, \mathbf{S}_1^{(n)}, \mathbf{S}_2^{(n)}\right) > \epsilon$ **do**
  $\mathbf{S}_0^{(n+1)} \leftarrow$ UPDATE_S_0 ($\mathbf{S}_0^{(n)}$, $\mathbf{S}_1^{(n)}$, $\mathbf{S}_2^{(n)}$)
  $\mathbf{S}_1^{(n+1)} \leftarrow$ UPDATE_S_1 ($\mathbf{S}_0^{(n+1)}$, $\mathbf{S}_1^{(n)}$, $\mathbf{S}_2^{(n)}$)
  $\mathbf{S}_2^{(n+1)} \leftarrow$ UPDATE_S_2 ($\mathbf{S}_0^{(n+1)}$, $\mathbf{S}_1^{(n+1)}$, $\mathbf{S}_2^{(n)}$)
  $n \leftarrow n + 1$
end while

$\mathbf{S}_0 \leftarrow \mathbf{S}_0^{(n)}$
$\mathbf{S}_1 \leftarrow \mathbf{S}_1^{(n)}$
$\mathbf{S}_2 \leftarrow \mathbf{S}_2^{(n)}$
return $\mathbf{S}_0$, $\mathbf{S}_1$, $\mathbf{S}_2$

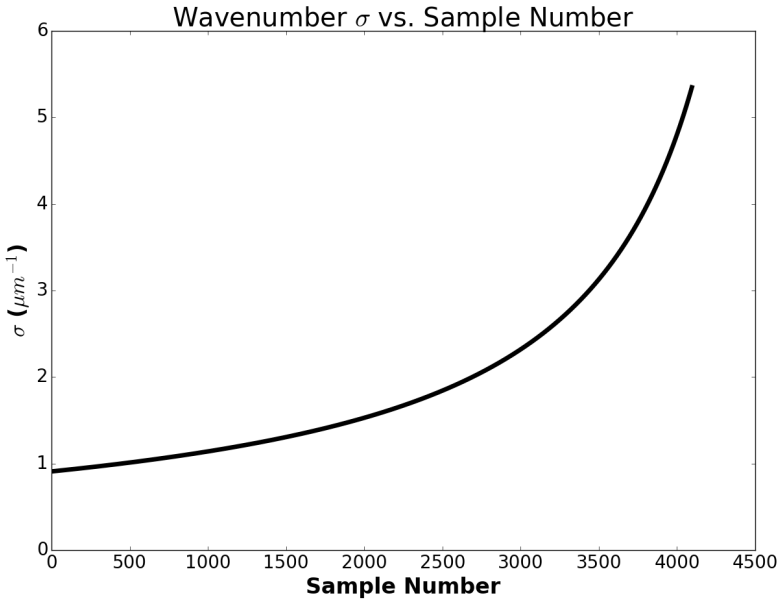

Figure 5.1. Wavenumber vs. sample number

and the Laplacians of the likelihood functions, diagonal matrices with entries

$$[\nabla^2_{\mathbf{S}_0} L(\mathbf{S}_0, \mathbf{S}_1, \mathbf{S}_2, \phi)]_{ii} = 1, \tag{4.35}$$

$$[\nabla^2_{\mathbf{S}_1} L(\mathbf{S}_0, \mathbf{S}_1, \mathbf{S}_2, \phi)]_{ii} = \cos^2(\phi_i), \tag{4.36}$$

and

$$[\nabla^2_{\mathbf{S}_2} L(\mathbf{S}_0, \mathbf{S}_1, \mathbf{S}_2, \phi)]_{ii} = \sin^2(\phi_i). \tag{4.37}$$

Algorithm 4.4 delineates the iterative reconstruction procedure for channeled spectropolarimetry. We minimize the overall cost, Eq. (4.24), by sequential updates of the Stokes parameters, until $c(\mathbf{S}_0, \mathbf{S}_1, \mathbf{S}_2)$ decreases to a certain value. Each update employs the gradient descent strategy in Algorithms 4.1–4.3. More generally, this alternating update procedure may aid reconstruction in nonlinear physical systems and nonlinear inverse problems, such as digital holography[11] or phase retrieval.[13,14]

5. COMPARISON OF RECONSTRUCTION RESULTS

In this section, we compare Fourier and iterative reconstruction, using the simulation from Section 3. The sample spectrum in Fig. 3.2, generated from the ground truth in Fig. 3.1, serves as our measurement $\mathbf{I}(\sigma)$. According to Eq. (4.19), the noise follows a Gaussian distribution; here we set

$$\mu = 0 \tag{5.1}$$

and

$$\sigma_n = 0.03. \tag{5.2}$$

For initialization, we input the Fourier reconstruction results from Fig. 3.4 and interpolate these results onto a non-uniformly spaced grid of wavenumbers to simulate a dispersive spectrometer. Iterative reconstruction can process these non-uniformly spaced samples without requiring interpolation. For reference, we plot the wavenumber for each sample in Fig. 5.1, which illustrates the non-linear spacing.

In this work, we assume the birefringence $B(\sigma)$ is known or can be measured, so that the phase $\phi(\sigma)$ in Eq. (2.7) is known with reasonable accuracy. In future work, we will incorporate the phase as a parameter to be updated in the iterative reconstruction procedure.

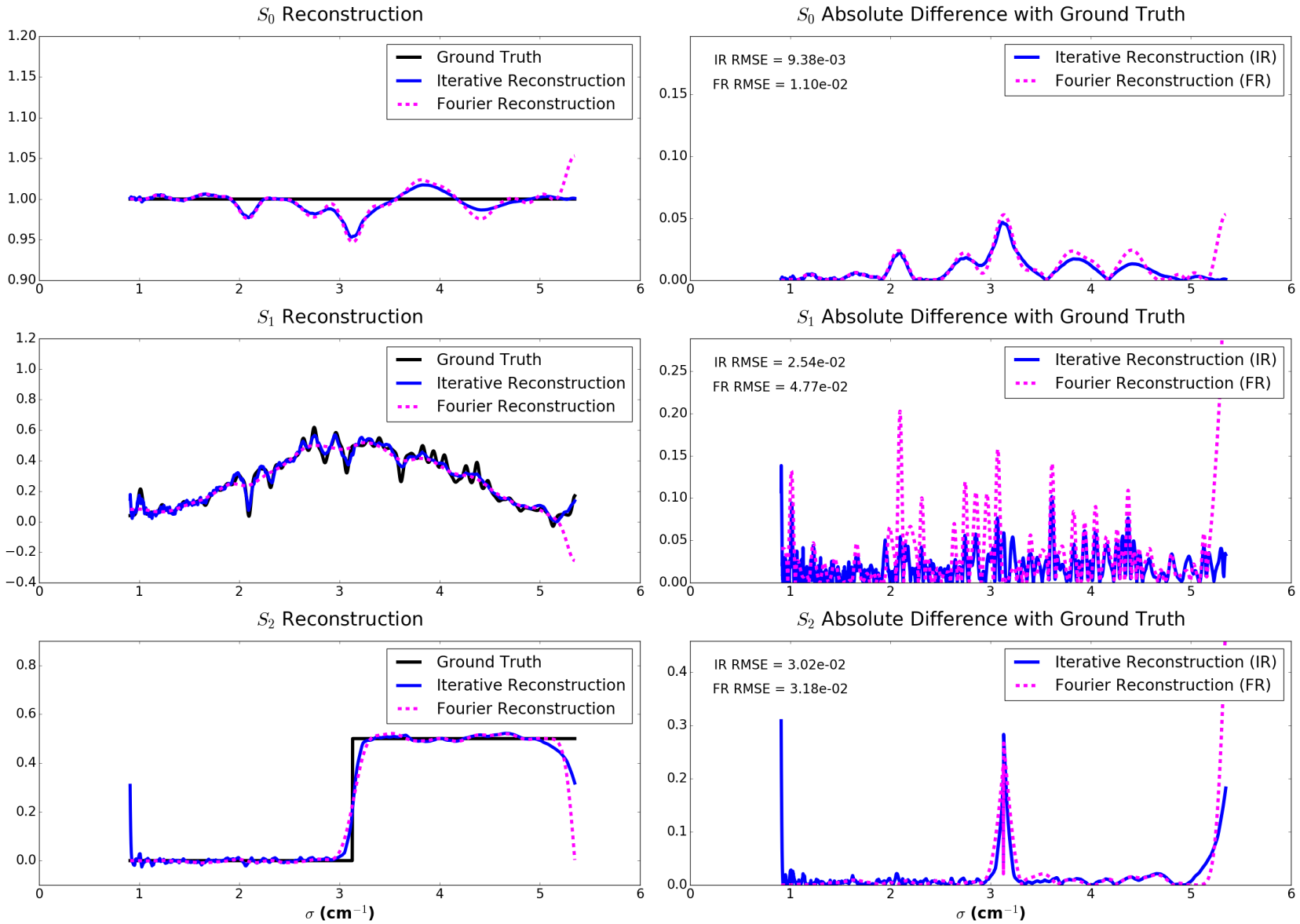

Figure 5.2. Comparison of ground truth, Fourier, and iterative reconstructions.

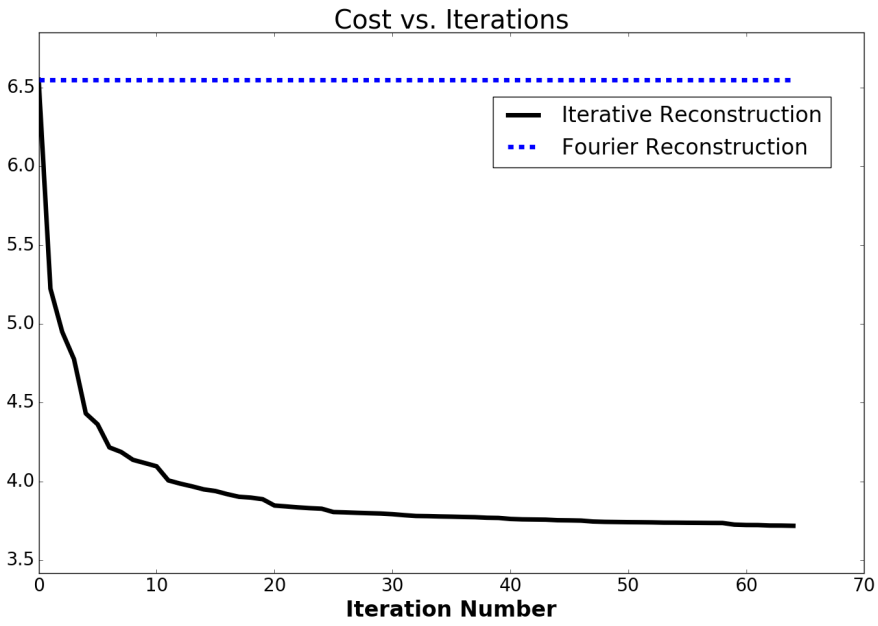

Figure 5.3. Cost vs. iterations.

Algorithm 4.4 iteratively updates the Stokes parameters, terminating when cost reduces to some threshold ϵ. We plot the end results in Fig. 5.2, with a comparison of ground truth and Fourier reconstruction. To quantify error, we compute the absolute difference between the ground truth and reconstructions and display the RSME for each technique. Looking at each parameter, we make the following observations:

- S_0 recovers its ideally flat signature more closely with iterative reconstruction.
- S_1 exhibits high frequency details, lost with Fourier reconstruction. Iterative reconstruction recovers these details.
- S_2 contains a step feature. Both the Fourier and iterative approaches produce similar reconstructions.

The iterative approach seems best at recovering low to intermediate frequency details, which might be typical in many applications. Noise degrades Fourier reconstruction by washing out details, as the recovery of the S_1 parameter in Fig. 5.2 demonstrates, but our iterative algorithm mitigates noise effects through regularization. On the other hand, very high frequency features, such as steps, seem to pose a challenge for both the Fourier and iterative methods, though these features may not be too common in practical test objects. Hence, *we can reconstruct signals that contain more bandwidth, an improvement over Fourier reconstruction.*

We can quantitatively measure reconstruction convergence by tracking the cost function, Eq. (4.24), for each iteration of Algorithm 4.4. Recall from Section 4 that this cost function includes a likelihood term that measures data fidelity and regularizer terms that penalize signal noise. The scalar regularizer terms, β_0, β_1, and β_2, are experimental parameters that can be tuned; we use values of $\beta_0 = 500$, $\beta_1 = 10$, and $\beta_2 = 50$. We compute the initial cost by evaluating $c(\mathbf{S}_0, \mathbf{S}_1, \mathbf{S}_2)$ using the Stokes parameters recovered from Fourier reconstruction. With each update in iterative reconstruction, indexed by n in Algorithm 4.4, we re-evaluate $c(\mathbf{S}_0, \mathbf{S}_1, \mathbf{S}_2)$ and plot the results in Fig. 5.3. The cost drops drastically, indicating convergence and agreeing with our observations of improved reconstruction.

6. CONCLUSION

We have proposed an iterative reconstruction algorithm to recover the Stokes parameters from channeled spectropolarimetric measurements. Our approach provides a framework for restoring CSP signals based on developing

a mathematical model of the physical system and minimizing a cost function. This general framework improves on standard Fourier transform processing: it recovers the Stokes parameters with better fidelity and more detail, processes samples that are non-uniformly spaced in wavenumber, reduces noise from environmental vibration and thermal fluctuations, does not assume the channels are band-limited, and quantifies reconstruction improvement through minimization of a cost function. Importantly, it can reconstruct signals that contain more bandwidth, an advancement over Fourier reconstruction. More generally, our alternating update strategy to solve for the Stokes parameters can be applied to other inverse problems or nonlinear physical systems. This work offers a significant improvement to Fourier reconstruction for channeled spectropolarimetry.

7. ACKNOWLEDGEMENTS

Sandia National Laboratories is a multi-program laboratory managed and operated by Sandia Corporation, a wholly owned subsidiary of Lockheed Martin Corporation, for the U.S. Department of Energy's National Nuclear Security Administration under contract DE-AC04-94AL85000.

REFERENCES

[1] M. W. Kudenov, M. J. Escuti, E. L. Dereniak, and K. Oka, "White-light channeled imaging polarimeter using broadband polarization gratings," Appl. Opt. **50**(15), 2283–2293 (2011).

[2] M. W. Kudenov and E. L. Dereniak, "Compact real-time birefringent imaging spectrometer," Opt. Express **20**(16), 17973–17986 (2012).

[3] D. E. Aspnes; Analysis of Semiconductor Materials and Structures by Spectroellipsometry. Proc. SPIE 0946, Spectroscopic Characterization Techniques for Semiconductor Technology III, 84 (August 9, 1988); doi:10.1117/12.947416.

[4] K. Oka and T. Kato, "Spectroscopic polarimetry with a channeled spectrum," Opt. Lett. **24**, 1475–1477 (1999).

[5] K. H. Nordsieck, "A simple polarimetric system for the Lick Observatory Image-Tube Scanner," Pub. Astron. Soc. Pac. 86(511) 324-329 (1974).

[6] M. W. Kudenov, N. A. Hagen, E. L. Dereniak, and G. R. Gerhart, "Fourier transform channeled spectropolarimetry in the MWIR," Opt. Express **15**(20), 12792–12805 (2007).

[7] P. R. Armstrong, E. B. Maghirang, F. Xie, F. E. Dowell, "Comparison of dispersive and Fourier-Transform NIR Instruments for Measuring Grain and Flour Attributes," Appl. Eng. Agric. **22**, 453 (2006).

[8] J. Hsieh, *Computed Tomography: Principles, Design, Artifacts, and Recent Advances* (SPIE, Bellingham, WA, 2003).

[9] C. F. LaCasse, R. A. Chipman, and J. S. Tyo, "Band limited data reconstruction in modulated polarimeters," Opt. Express **19**(16), 14976–14989 (2011).

[10] J. Craven-Jones, B. M. Way, M. W. Kudenov, and J. A. Mercier, "Athermalized channeled spectropolarimetry using a biaxial potassium titanyl phosphate crystal," Opt. Lett. **38**(10), 1657–1659 (2013).

[11] D. J. Lee, C. A. Bouman, and A. M. Weiner, "Single shot digital holography using iterative reconstruction with alternating updates of amplitude and phase," in *IS&T Electronic Imaging: Computational Imaging XIV Proceedings* (Society for Imaging Science and Technology, 2016), pp. 158.1–158.6.

[12] S. Boyd and L. Vandenberghe, *Convex Optimization* (Cambridge University Press, 2004).

[13] D. J. Lee and A. M. Weiner, "Optical phase imaging using a synthetic aperture phase retrieval technique," Opt. Express **22**, 9380–9394 (2014).

[14] D. J. Lee, K. Han, H. J. Lee, and A. M. Weiner, "Synthetic aperture microscopy based on referenceless phase retrieval with an electrically tunable lens," Appl. Opt. **54**, 5346–5352 (2015).